Tracking small UAVs using a Bernoulli filter

David R. Cormack
School of Engineering and Physical Sciences
Heriot-Watt University
Edinburgh
EH14 4AS, UK
drc9@hw.ac.uk

Daniel E. Clark
School of Engineering and Physical Sciences
Heriot-Watt University
Edinburgh
EH14 4AS, UK
D.E.Clark@hw.ac.uk

***Abstract*—The necessity for maintaining surveillance in airborne environments is ever growing. Criminals and terrorists are finding new and elaborate means of attack, and small UAVs such as quadcopters and hexacopters could be a possible threat. Their small size and agile movement will make them difficult to detect. This work aims to determine whether or not these small UAVs can be detected at short range using radar, and if so, track them over time using a suitable filter such as a Bernoulli filter.**

***Index Terms*—Bernoulli, filter, radar, UAV, quadcopter, hexacopter, tracking**

I. Introduction

Over the last five to ten years, there have been many new developments in the field of small UAVs, namely quadcopters and hexacopters [1]. Many of these units are readily available to hobbyists and amateur pilots from many electronics stores on the high street [2], [3]. With their small size and agile movement, these small UAVs could pose a major threat to defence and security [4]. A number of high-profile news stories have highlighted this potential threat, such as the spying on French landmarks, the inciting of a riot at a football match in Serbia, and the UAV that crashed into seating at the US Open tennis in New York in 2015 [5]–[7]. The major issue surrounding these small UAVs is their detectability using a reliable sensor. All of these threats could have been avoided, had the small UAVs been detected and tracked at an early stage, and countermeasures set in motion.

Radar tracking works best with a low density of targets, and each target moves with a predictable dynamical model. A number of environmental factors can have an effect on the accuracy of tracking, such as the weather conditions and the terrain that surrounds the target. These tracking methods may encounter various problems when either a very large number of detections are gained, or a limited number from a small target for example. These small targets may be difficult to distinguish from the clutter around them.

This paper will introduce one method of detecting and tracking a small UAV over time, using a radar developed by Leonardo, and a Bernoulli Gaussian Sum filter [8]. Section II will give a background to the small UAVs in question, including how detectable they should be to radar. Section III will discuss the test that was set up in order to gain real data sets for use in the tracking algorithm. Section IV introduces the Bernoulli filter and it's implementation, with the results shown in Section V.

II. Small UAVs/Quadcopters

The defence sector currently have an interest in detecting these small UAVs, and developing safe countermeasures to bring them down if they pose a threat [9]. As the UAVs are almost invisible to the naked eye at distances further than 300 metres, a suitable sensor such as radar will be required to detect them at further ranges. Their detectability is based on the theory of Radar Cross Section [10]. If all of the radar energy focused on the target was reflected evenly in all directions, the RCS would be equal to the target's cross-sectional area with respect to the radar. In this application however, some of the energy will be absorbed by the UAV's structure, and the reflected energy will not distribute evenly in all directions. The value of RCS will vary for a target, depending on factors such as the material it is made from, and its orientation with respect to the radar. The structure of a target can also amplify radar returns in particular detections if a signal bounces multiple times within the structure before being deflected away. Right angles are particularly good at doing this.

As an initial assessment of how detectable this type of UAV is, a widely-available quadcopter was placed inside a large anechoic chamber at Leonardo in Edinburgh, UK. The quadcopter that was used is the DJI Phantom II [11]. It is widely available in many electronics stores. The output RCS plot for this UAV is shown in Fig. 1. The structure of the quadcopter can be seen, with strong reflections coming from the front of the object as expected. In order to build up this RCS plot, the quadcopter was placed on top of a polystyrene plinth and rotated through 360° in increments of 0.25°. At each increment, a burst of RF energy is directed towards the UAV and the strength of the returned signal is measured. This intensity in dB is then plotted, with hotter colours indicating stronger returns. The testing was performed across a frequency range between 6 GHz and 18 GHz to give coverage in both the X-band and Ku-band. The RCS varying with the target's orientation to the radar, and the RCS varying with the transmission frequency can be seen in Fig. 2 and Fig. 3 respectively.

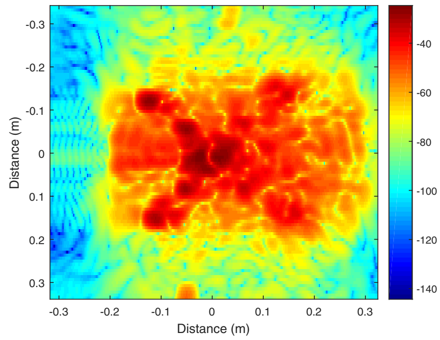

Fig. 1. RCS plot for DJI Phantom II Quadcopter. The RCS at each point on the plot has been frequency-averaged between 6 GHz and 18 GHz to give the result. The colour scale is given in dBsm. [12].

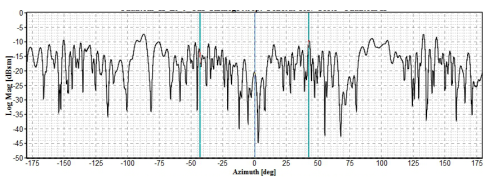

Fig. 2. RCS varying with target orientation. The green vertical lines show -45° and +45°. Again the resultant RCS has been frequency-averaged between 6 GHz and 18 GHz. [12].

It was found that the peak RCS value gained during this test was -24.6dBsm. Using this value in a form of the radar range equation,

$$\sqrt[4]{\frac{P_t \tau G^2 \sigma \lambda^2}{4\pi^3 k T_s L(SNR)}} \tag{1}$$

where P_t is the peak transmit power in Watts, τ is the pulse duration, G is the radar's gain, σ is the RCS of the target, λ is the radar's operating wavelength, k is the Boltzmann constant, T_s is the system noise temperature and L is the overall system loss in decibels, it is possible to determine the maximum range that the UAV should be detectable at. This was calculated to be approximately 1.2 kilometres using a specification of a variant of the PicoSAR radar which is designed and manufactured by Leonardo. More information about this radar will be given in Section III.

III. Trial Setup

In order to test the theory, a ground trial was set up to see if these small UAVs would be detectable using AEXAR, an experimental variant of the Leonardo PicoSAR radar [13]. It has

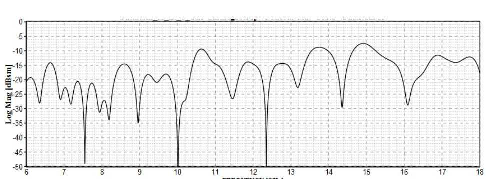

Fig. 3. RCS varying with radar transmission frequency. The turntable is kept static at 0° and the transmission frequency is varied to give the result. [12].

Fig. 4. DJI Inspire I Quadcopter [14].

Fig. 5. DJI S900 Hexacopter [15].

a larger array antenna than the standard radar, and transmits more power, making it more likely to detect smaller targets, especially at shorter ranges. The quadcopter and hexacopter used as a part of this trial are not the same as the one used in the anechoic chamber experiment, so the RCS result and the maximum range calculation can only be inferred as an estimate. The UAVs used can be seen in Figures 4 and 5. The data collected during this trial has then been used to develop the tracking method described later in Section IV.

The trial was performed on the 20th of August 2015, at East Fortune Airfield in East Lothian, GB. The radar was located inside the back of a van, which was positioned at the West end of the runway. The UAVs and their pilot were located 1 kilometre away at the other end of the runway. The radar was kept in its fixed position mode with a scan pattern between -6° and +6°. In order to gain a reading for the background noise and clutter in the surveillance region, a null test was performed. The UAVs were initially flown in a linear motion towards and away from the radar, in order to gain a maximum Doppler shift and to detect the target outside of the main beam clutter region. After completing these tests, the UAVs were flown in a much more random pattern inside the surveillance region, including circular paths and tight agile turns. A number of different radar waveforms were used, including changes to the Pulse Repetition Frequency and Chirp Bandwidth of the transmitted signal.

IV. Bernoulli Filtering

The Bernoulli filter, also known as a joint target-detection and tracking (JoTT) filter [16], can be seen to be the optimal Bayes filter for a single dynamic target that can randomly appear and disappear from the surveillance region in question. The key to this type of filtering is the inclusion of the existence binary random variable. The Bernoulli Random Finite Set formulation is different to that of traditional approaches, in that the state is treated as its own set, rather than a vector.

Further work has been carried out in the area of Bernoulli filtering, such as the use of data from multiple sensors to gain a more accurate track on a single target [17] and the development of a multi-Bernoulli filter to track multiple targets at the same time [18].

The model used in this simulation is that of the detector output measurements for point targets [8]. It is assumed that at each time step, the target in question will generate one single detection and all other detections at that time will be assumed to be false alarms. The number of false alarms will be assumed to be modelled by the Poisson distribution.

A. Filter Equations

1) Prediction: With the inclusion of the probability of existence variable, it must also be predicted and updated at each time step. The prediction equation can be shown to be,

$$q_{k|k-1} = p_b(1 - q_{k-1|k-1}) + p_s q_{k-1|k-1} \tag{2}$$

where p_b is the probability of target birth, and p_s is the probability of target survival. This equation effectively states that a predicted target could come from a new birth, such as a target entering the surveillance region, or from a target surviving from the previous time step. When implementing this kind of filter, it will be assumed that there will be a linear Gaussian transition, likelihood and birth model, with both the probability of detection and the probability of survival being constant. The birth model $b_{k|k-1}(x)$ is expressed as a single Gaussian of the form

$$w_{b,k}\mathcal{N}(x; m_{b,k}, Q_{b,k}) \tag{3}$$

where, $w_{b,k}$ represents the birth weights, $m_{b,k}$ represents the birth mean positions and $Q_{b,k}$ represents the birth position covariance. The prediction equations will follow those of a basic Kalman filter. The predicted spatial PDF can also be expressed as a Gaussian sum of the form,

$$s_{k|k-1}(x) = \sum_{i=1}^{N_{k|k-1}} w_{k|k-1}^{(i)}\mathcal{N}(x; m_{k|k-1}^{(i)}, P_{k|k-1}^{(i)}) \tag{4}$$

where $w_{k|k-1}^{(i)}$ are the predicted weights, $m_{k|k-1}^{(i)}$ are the predicted means and $P_{k|k-1}^{(i)}$ are the predicted covariances. The sum of the weights must be equal to 1.

2) Update: The update equations for this type of Bernoulli filter make use of those found in the update stage of a basic Kalman filter. The equation used for updating the probability of existence is,

$$q_{k|k} = \frac{1 - \Delta_k}{1 - q_{k|k-1}\Delta_k} q_{k|k-1} \tag{5}$$

where,

$$\Delta_k = p_D \left[1 - \sum_{z \in Z_k} \sum_{i=1}^{N_{k-1}} \frac{w_{k-1}^{(i)} q_k^{(i)}(z)}{\lambda_c c(z)}\right] \tag{6}$$

$c(z)$ is the density of the Poisson clutter process and λ_c is the clutter rate.

The update equation for the spatial PDF is,

$$s_{k|k}(x) = \frac{(1 - p_D)}{1 - \Delta_k} s_{k|k-1}(x) + \frac{p_D}{1 - \Delta_k} \times \sum_{z \in Z_k} \sum_{i=1}^{N_{k|k-1}} \frac{w_{k|k-1}^{(i)} q_k^{(i)}(z)}{\lambda_c c(z)} \mathcal{N}(x; m_{k|k}^{(i)}, P_{k|k}^{(i)}) \tag{7}$$

where,

$$q_k^{(i)}(z) = \mathcal{N}(z; \eta_{k|k-1}^{(i)}, S_{k|k-1}^{(i)}),$$
$$\eta_{k|k-1}^{(i)} = J m_{k|k-1}^{(i)},$$
$$S_{k|k-1}^{(i)} = J P_{k|k-1}^{(i)} J^T + R_k,$$
$$m_{k|k}^{(i)} = m_{k|k-1}^{(i)} + K_k^{(i)}(z - \eta_{k|k-1}^{(i)}),$$
$$P_{k|k}^{(i)} = P_{k|k-1}^{(i)} + K_k^{(i)} J P_{k|k-1}^{(i)},$$
$$K_k^{(i)} = P_{k|k-1}^{(i)} J^T [S_{k|k-1}^{(i)}]^{-1},$$

and J is a Jacobian matrix.

B. Practical Implementation

The probability of detection p_D was set to 0.99 and the probability of target birth p_b to 0.1. A large number of false alarms were being generated by trees swaying in the wind, and from vehicles moving around at the sides of the runway. The clutter rate λ_c has been set at 5 per scan. Due to the radar's position being stationary during the course of the trial, conventional methods of reducing the angular uncertainty such as were not available. The radar was operating at its higher bandwidth and digitiser rate, meaning that more samples were being taken in range, and therefore reducing the uncertainty in this dimension. Both of these uncertainties have been built into the model.

After the model has been declared and set up, the radar measurements are read in. For each detection gained, such as the one highlighted in Fig. 6, the radar will generate a target report that contains relevant information such as the target's position with respect to the radar. Data from each of these reports can be read in as a measurement z, which is stored in Z_k, where k is the time step. As the radar platform is kept stationary, it will be assumed that it is located at $(0, 0, 0)$ in the XYZ Cartesian space. Each measurement z will have the form,

$$[r, \dot{r}, \phi, \theta]'$$

where r is the range, $\dot{r}$ is the range rate, ϕ is the azimuthal angle and θ is the elevation angle. The state vector X will contain 6 elements and be defined as,

$$[x, \dot{x}, y, \dot{y}, z, \dot{z}]'$$

where x, y, z are the positions and $\dot{x}, \dot{y}, \dot{z}$ are the velocities with respect to each axis. One Gaussian birth term will be used at each time-step and will have a large initial covariance in order to deal with the high number of false alarms. In this scenario, no measurements are initially available at the first time-step, so the initial probability of existence will be set at a value of 0.98.

The update stage has been built with the inclusion of the Extended Kalman filter equations to account for any non-linearities. Standard elimination and pruning schemes have been included to reduce the number of Gaussian components. The merging function uses the Hellinger distance [19] to determine whether Gaussians are located close enough to each other.

Algorithm 1 Prediction stage

given $\{w_{k-1}^{(i)}, m_{k-1}^{(i)}, P_{k-1}^{(i)}\}_{i=1}^{N_{k-1}}$

  $q_{k-1|k-1} = q_{k|k-1}$
  $q_{k|k-1} = p_b(1 - q_{k-1|k-1}) + (1 - p_D)q_{k-1|k-1}$
  procedure PREDICTION FOR BIRTH TARGETS
    $i = 0$
    for $j = 1, \ldots, N_{\gamma,k}$ **do**
      $i = i + 1$
      $w_{k|k-1}^{(i)} = \frac{w_{\gamma,k}^{(j)} p_b(1-q_{k-1|k-1})}{q_{k|k-1}}$
      $m_{k|k-1}^{(i)} = m_{\gamma,k}^{(j)}$
      $P_{k|k-1}^{(i)} = P_{\gamma,k}^{(j)}$
    end for
  end procedure
  procedure PREDICTION FOR EXISTING TARGETS
    for $j = 1, \ldots, N_{k-1}$ **do**
      $i = i + 1$
      $w_{k|k-1}^{(i)} = \frac{(1-p_D)q_{k-1|k-1}}{q_{k|k-1}} w_{k-1}^{(j)}$
      $m_{k|k-1}^{(i)} = F_{k-1} m_{k-1}^{(j)}$
      $P_{k|k-1}^{(i)} = F_{k-1} P_{k-1}^{(j)} F_{k-1}^T + Q_{k-1}$
    end for
    $N_{k|k-1} = i$
  end procedure

Algorithm 2 Update stage

  procedure UPDATE
    for $j = 1, \ldots, N_{k|k-1}$ **do**
      $m_k^{(j)} = m_{k|k-1}^{(j)}$
      $P_k^{(j)} = P_{k|k-1}^{(j)}$
    end for
    for $z \in Z_k$ **do**
      for $j = 1, \ldots, N_{k|k-1}$ **do**
        $K_k^{(j)} = P_{k|k-1}^{(j)} J^T (S_{k|k-1}^{(j)})^{-1}$
        $m_k^{(\ell N_{k|k-1}+j)} = m_{k|k-1}^{(j)} + K_k^{(j)}(z - \eta_{k|k-1}^{(j)})$
        $P_k^{(\ell N_{k|k-1}+j)} = P_{k|k-1}^{(j)} - K_k^{(j)} J (P_{k|k-1}^{(j)})^T$
        $\hat{w}_k^{(j)} = w_{k|k-1}^{(j)} \mathcal{N}(z; \eta_{k|k-1}^{(j)}, S_{k|k-1}^{(j)})$
      end for
    end for
    if $Z_k = \emptyset$ **then**
      $\Delta_k = p_D$
      $q_{k|k} = \frac{1-\Delta_k}{1-q_{k|k-1}\Delta_k} q_{k|k-1}$
      for $j = 1, \ldots, N_{k|k-1}$ **do**
        $w_k^{(j)} = \frac{(1-p_D)}{1-\Delta_k} w_{k|k-1}^{(j)}$
      end for
    else
      $\Delta_k = p_D(1 - \sum_{i=1}^{N_{k|k-1}} \hat{w}_k)$
      $q_{k|k} = \frac{1-\Delta_k}{1-q_{k|k-1}\Delta_k} q_{k|k-1}$
      $n = N_{k|k-1}$
      for $j = 1, \ldots, N_{k|k-1}$ **do**
        $w_k^{(j)} = \frac{(1-p_D)}{1-\Delta_k} w_{k|k-1}^{(j)}$
      end for
      for $z \in Z_k$ **do**
        for $j = 1, \ldots, N_{k|k-1}$ **do**
          $n = n + 1$
          $w_k^{(n)} = \frac{p_D}{1-\Delta_k} \hat{w}_k^{(\ell N_{k|k-1}+j)}$
        end for
      end for
    end if
    $N_k = \ell N_{k|k-1} + N_{k|k-1}$
  end procedure

output $\{w_k^{(i)}, m_k^{(i)}, P_k^{(i)}\}_{i=1}^{N_k}$

V. RESULTS

As can be seen in Fig. 6, the small UAV is successfully detected by the radar. It appears as the bright flash to the right of the main beam clutter region. In Fig. 7 and Fig. 8, the + symbols represent the detections that have been recorded by the radar, and the o symbols represent the estimates that have been given out from the filter. It can be seen in Fig. 8 that the Bernoulli filter provides very accurate track on the target in the Y-axis. This variation in Y-coordinate correlates with the flight path taken by the pilot on the day, directly towards and away from the radar. The discontinuity that appears at approximately time step 80 is due to the UAV decelerating quickly to a hover. The filter coasts its estimates for a number of time steps and then detects the UAV again successfully. In both Fig. 7 and Fig. 8, there are a number of detections that do not lie on the target track. These are generated due to clutter such as trees swaying in the wind, and also targets that are not of interest, such as farm vehicles working in a nearby field.

VI. CONCLUSIONS

The Bernoulli Gaussian Sum filter has successfully given sensible estimates of the UAVs position and tracked it over time. The filter has dealt with the false alarms that are present at close range.

VII. ACKNOWLEDGMENTS

The authors thank Dr. David Greig, Dr. Anthony Swain and Andrew Glass in the Systems Engineering department at Leonardo, Edinburgh for their time and contribution to this project. This includes the funding to carry out the radar trial in the field, the use of the AEXAR radar, and the radar data used to develop the Bernoulli filter.

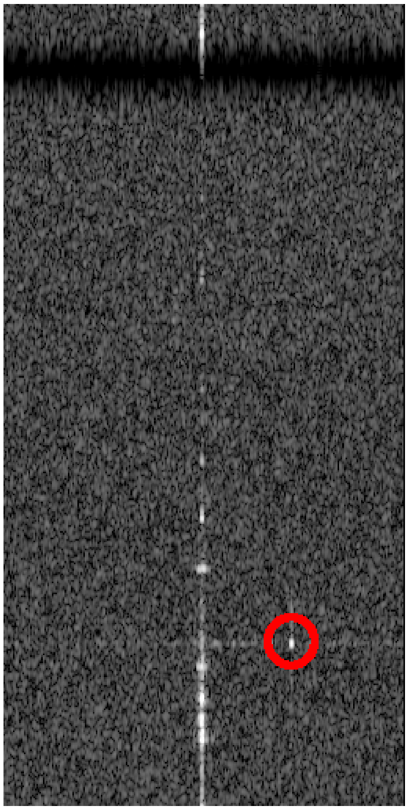

Fig. 6. Detection highlighted on range/Doppler map [12].

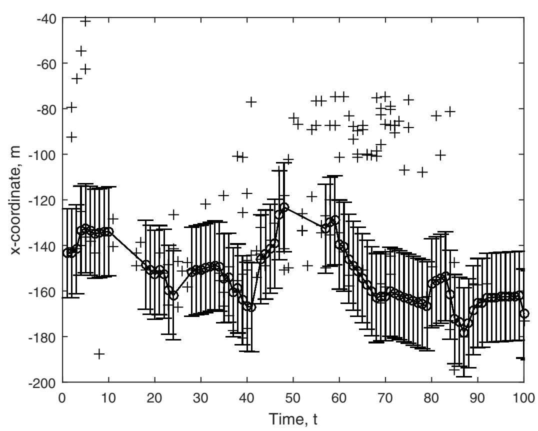

Fig. 7. X coordinates of detections and estimates plotted over time. [12].

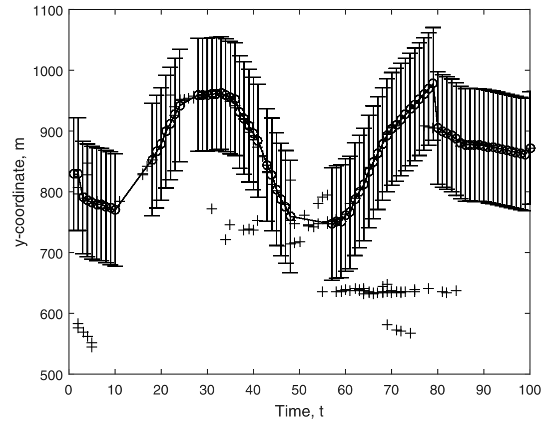

Fig. 8. Y coordinates of detections and estimates plotted over time. [12].

References

[1] DroneBuff, "What's the best quadcopter?" November 2015. [Online]. Available: http://dronebuff.com/whats-best-quadcopter/

[2] Maplin, "Radio Controlled Drones — Maplin," March 2016. [Online]. Available: http://www.maplin.co.uk/c/gadgets-toys-and-hobbies/radio-controlled/radio-controlled-drones

[3] Menkind, "Drones, Quadcopters and Quadrotor — Menkind," March 2016. [Online]. Available: http://www.menkind.co.uk/remote-control/drones-quadcopters

[4] BBC, "Warning over drones use by terrorists," January 2016. [Online]. Available: http://www.bbc.co.uk/news/technology-35280402

[5] D. Mail, "New terror alert for France after 'at least' five drones are spotted flying above paris landmarks including Eiffel Tower and the US Embassy," February 2015. [Online]. Available: http://www.dailymail.co.uk/news/article-2966482/New-terror-alert-France-five-drones-spotted-flying-Paris-landmarks-including-Eiffel-Tower-embassy.html

[6] BBC, "Serbia v Albania: Drones, flags and violence in abandoned match," October 2014. [Online]. Available: http://www.bbc.co.uk/sport/football/29624259

[7] ——, "US Open: New York teacher arrested after drone crashes into stands," September 2015. [Online]. Available: http://www.bbc.co.uk/news/world-us-canada-34155773

[8] B. Ristic, B. Vo, B. Vo, and A. Farina, "A Tutorial on Bernoulli filters: Theory, Implementations and Applications," *IEEE Transactions on Signal Processing*, vol. 61, pp. 3406–3430, 2013.

[9] Finmeccanica, "Finmeccanica - Selex ES launches Falcon Shield Counter-UAV system," September 2015. [Online]. Available: http://www.finmeccanica.co.uk/-/falcon-shield-launch

[10] RadarTutorialEU, "Radar Basics - Radar Cross Section," March 2016. [Online]. Available: http://www.radartutorial.eu/01.basics/Radar%20Cross%20Section.en.html

[11] DJI, "Phantom 2 - The Spirit of Flight — DJI," February 2016. [Online]. Available: http://www.dji.com/product/phantom-2

[12] D. R. Cormack, "Tracking of Difficult Targets in a Challenging Environment," Master's thesis, School of Engineering and Physical Sciences, Heriot-Watt University, 2015.

[13] Finmeccanica, "PicoSAR - Detail," March 2016. [Online]. Available: http://www.finmeccanica.com/en/-/picosar-1

[14] D. Wiki, "Inspire 1 - DJI Wiki," August 2015. [Online]. Available: http://wiki.dji.com/en/index.php/Inspire-1

[15] DJI, "Spreading Wings S900 - Highly portable, powerful aerial system for the demanding filmmaker — DJI," August 2015. [Online]. Available: https://www.dji.com/product/spreading-wings-s900

[16] R. P. Mahler, "Statistical Multisource-Multitarget Information Fusion," 2007.

[17] B. Vo, C. See, N. Ma, and W. Ng, "Multi-Sensor Joint Detection and Tracking with the Bernoulli filter," *IEEE Transactions on Aerospace and Electronic Systems*, vol. 48, pp. 1385–1402, 2012.

[18] B. Vo, B. Vo, R. Hoseinnezhad, and R. Mahler, "Robust Multi-Bernoulli Filtering," *IEEE Journal of Selected Topics in Signal Processing*, vol. 7, pp. 399–409, 2013.

[19] S. Nagappa, D. Clark, and R. Mahler, "Incorporating Track Uncertainty into the OSPA Metric," in *2011 Proceedings of the 14th International Conference on Information Fusion (FUSION)*, 2011.